A GRANULAR ASSEMBLY SIMULATION FOR THE SEISMIC LIQUEFACTION OF SAND

By Motohiko HAKUNO* and Yuji TARUMI**

Various liquefaction analyses have been made. No numerical liquefaction analysis in which sand is considered a non-continuous material, however, has yet been reported. In 1971, the Distinct Element Method (DEM) was introduced by Cundall. This method is a numerical simulation by which rock behavior is analyzed based on the assumption that individual rock elements satisfy the equation of motion. We developed a modified DEM that takes into account pore water pressure based on Darcy's law. We analyzed the liquefaction of saturated sand under seismic excitation. Excessive pore water pressure in the numerical results rose gradually due to the effect of shaking. This result agrees with results of past laboratory tests.

Keywords : sand liquefaction, Distinct Element Method (DEM)

1. INTRODUCTION

Various kinds of liquefaction analysis have been done in laboratory experiments and using the Finite Element Method (FEM). But, almost no numerical liquefaction analysis in which sand has been considered a noncontinuous material has yet been reported.

The idea of handling the sand analytically as a granular assembly was introduced by T. Mogami[1] in 1965. In 1971, the Distinct Element Method (DEM) was introduced by Cundall[2], a numerical simulation used to analize the behavior of rock based on the assumption that each individual rock element satisfies the equation of motion. Independent of Cundall's research, Hakuno and Hirao also conducted a granular assembly simulation of circular particles in their investigation of the static deformation problem of sand[3]. In 1983, Kiyama, Fujimura and Nishimura[4] used Cundall's method to estimate settlement of the ground surface during the construction of a tunnel based on the assumption that particles in the ground are circular. They also analyzed the behavior of grain particles in a silo during the extrusion of the particles through a hole[5]. These analyses were made for particle elements with the same radii, several hundreds of particles being analyzed.

Uemura and Hakuno[6] modified the DEM by introducing a restitution coefficient then applied it to the dynamic analysis of a soil model with more than 3 000 circular elements of different radii. Izutsu, Kiyama, Fujimura and Nishimura[7] conducted a granular assembly simulation taking into account the pore water effect ; but, in their research the particles did not undergo relative displacement. Therefore, the behavior of particles produced by a change in pore pressure could not be described. Kishino[8] also treated the static properties of pore water pressure using a granular assembly simulation method different from the DEM,

---

* Professor, Earthquake Research Institute, University of Tokyo (Yayoi 1-1-1 Bunkyo-ku, Tokyo)
** Civil Engineer, Japan Public Highway Corporation (Kasumigaseki 3-3-2 Chiyoda-ku, Tokyo)

but his method treats only the static problem.

In the analyses described above, the pore water between particles was not accounted for in the dynamic liquefaction problem. Therefore, we have developed a modified DEM using Darcy's law that takes into account the pore water pressure[9]. We analyzed the liquefaction of saturated sand under seismic excitation. The assembly model consists of circular elements, with log-normal distributed radii, and it is packed by dropping.

2. PORE WATER BETWEEN SAND PARTICLES

(1) Dividing the space between particles

The pore pressure between particles is not taken into account in the conventional DEM. We have now developed a modified DEM that does take it into account. It is first necessary to divide the space between particles into a proper polygon which delineates that space and to obtain its area. An example of divided polygons in a particle assembly is shown in **Fig. 1**. The area of the shaded parts (actual area of the pore spaces) can be obtained by subtracting the sum of the fan-shaped areas from the area of the polygon. In this process, the overlapping area of two particles is neglected because it is very small. Even if a particle moves a small distance, the structure of the polygon does not change.

Once a constitution diagram of such polygons, (**Fig. 2**) has been prepared, it is not necessary to repeat the process at each time step; Only calculation of the pore space area is required. Rearrangement of the constitution diagram is necessary after several calculations because the locations of the particles change markedly.

(2) Calculation of the pore pressure

When considering the pore water between particles, various forces acting on the particle (the pore pressure, inertial force of water, etc.) should also be considered. Pore pressure is the only force considered in the simulation presented here. It is divided into static water and excessive water pressures (the latter being the dynamic water pressure), and the pore spaces are assumed to be saturated with water. The static water pressure is accounted for by subtracting the buoyancy force from the weight of the particle.

The excessive pore water pressure is obtained as follows: First, water is assumed to be an elastic medium without shear resistance. The area of pore K is expressed by A_k, and the area of the confined water corresponding to the excessive pore pressure being zero in the pore K by W_k. From the volume elastic constant of water, E_w, and the strain of the water area

$$\delta W = (W_k - A_k)/W_k,$$

the excessive water pressure, U_k is

$$U_k = E_w \cdot \delta W \cdots\cdots\cdots (1)$$
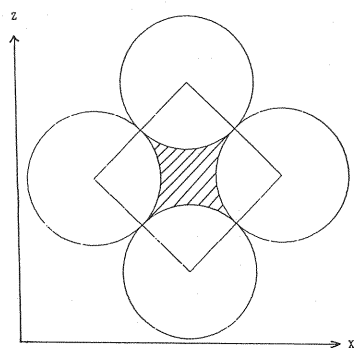
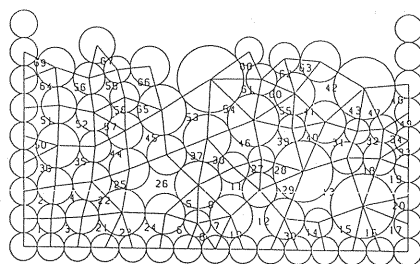When $W_k = A_k$ (Initial stable condition),

Fig. 1 Coordinates of Particles.

Fig. 2 Numbering of pore figures.

$$U_k = 0 \cdots\cdots\cdots (2)$$

The value of A_k varies according to the motion of the particles because of the force acting on them.

Pore pressures between neighboring particles differ from pore to pore. Water will move to the pore with the lower pressure, and W_k and U_k will change accordingly. U_k is a two-dimensional, isotropical load that is positive in the case of compression and negative in the case of tension. This U_k next is resolved into the forces acting on each particle. **Fig. 3** illustrates how the U_k acts on a particle, i. FU_kX_i, the component on the X coordinate, and FU_kZ_i, the component on the Z coordinate, for the water pressure acting on particle i can be calculated by the following equation.

$$\left. \begin{aligned} FU_kX_i &= \int_{\alpha_1}^{\alpha_2} -U_k r_i \cos\theta d\theta = -U_k r_i (\sin\alpha_2 - \sin\alpha_1) \\ FU_kZ_i &= \int_{\alpha_1}^{\alpha_2} -U_k r_i \sin\theta d\theta = -U_k r_i (\cos\alpha_2 - \cos\alpha_1) \end{aligned} \right\} \cdots\cdots (3)$$

This is the pore pressure on particle i from pore K; consequently, the total pressure on particle i is the summation of the pressures from the pore belonging to that particle.

(3) Water flow to another pore

Water in a pore moves to the neighboring pore when the excessive pore pressure changes. This produces a difference in pore pressure in the neighboring pore, and a small amount of water moves to that pore.

As shown in **Fig. 4** (a), the contact condition of particles i and j is expressed in equation (4),

$$r_i + r_j + \varepsilon_m \geq R_{ij} \cdots\cdots (4)$$

Furthermore, the pore condition is

$$r_i + r_j + l_m \geq R_{ij} \cdots\cdots (5)$$

It is assumed that a water pressure difference occurs between pores K and L and that the amount of water W', flows from K to L (**Fig. 4**(b)). On the assumption that the water pressures U_K and U_L become equal in the next calculation step, we obtain

$$\frac{U_K'}{E_w} = \frac{W_K - W' - A_K}{W_K - W'} = \frac{U_L'}{E_w} = \frac{W_L + W' - A_L}{W_L + W'} \cdots\cdots (6)$$

Its solution is given in (7).

$$W' = \frac{A_L W_K - A_K W_L}{A_K + A_L} \cdots\cdots (7)$$

Defining the water pressure gradient I_{KL}, which becomes non-dimensional, by dividing the water pressure difference for pores K and L by E_w, we obtain

$$I_{KL} = \frac{U_K - U_L}{E_w} = \frac{A_L W_K - A_K W_L}{W_K W_L} \cdots\cdots (8)$$

Further, by assuming that $A_{KL} = W_K W_L / (A_K + A_L)$, W' is expressed by equation (9).

$$W' = A_{KL} I_{KL} \cdots\cdots (9)$$

From equations (6)-(9), the flow amount, q_{KL}, from pore K to L can be expressed as

$$q_{KL} = K A_{KL} I_{KL} \cdots\cdots (10)$$

in which K is the permeability coefficient. Eq. (10) is a two dimensional expression of Darcy's law when no
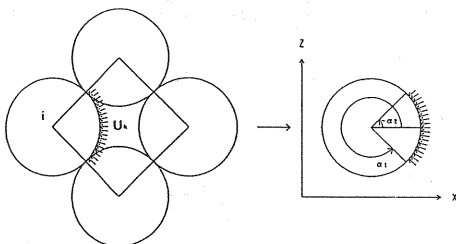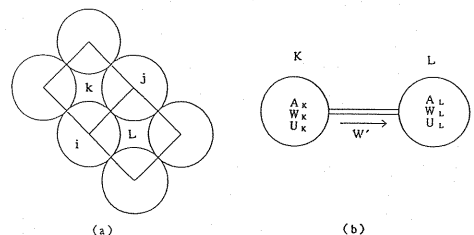

Fig. 3　Modeling of excessive pore water pressure.

Fig. 4　Diagram of two neighboring pores.

potential head is considered. The quantity of water, W_K, in pore K at time t is

$$[W_K]_t = [W_K]_{t-\Delta t} + \sum KA_{KL}I_{KL}\Delta t \quad\cdots\cdots\cdots (11)$$

in which, is the sum of all the pores, L, surrounding pore K. If two particles are in contact, water can not move through the contact point in the two-dimensional case. Whereas, in the three dimensional case, water can easily move through the point near the contact. We therefore adopted the following two values for the permeability coefficient, K, based on conditions (4) and (5),

$$K = K_1 \quad\cdots\cdots\cdots (12 \cdot a)$$

  when $R_{ij} - l_m \leq r_i + r_j + \varepsilon_m < R_{ij}$

$$K = K_2 \quad\cdots\cdots\cdots (12 \cdot b)$$

  when $R_{ij} \leq r_i + r_j + \varepsilon_m$

Case (12·b) corresponds to the point-to-point contact of two particles.

3. SPRING CONSTANTS

Spring constants between particles K_n in the normal and K_s in tangential direction have to be assumed before analysis. Kiyama and Fujimura determined the values of spring constants using a contact theory for an elastic cylinder. When two cylinders (of radii, r_1, r_2) with same Young's modulus E and Poison's ratio, ν are compressed with a load, q, per unit depth, the approaching displacement, δ, and the contact width, b, are given in eq. (13·a–b)

$$\delta = \frac{2(1-\nu^2)q}{\pi E}\left(\frac{3}{2} + \ln\frac{4\,r_1}{b} + \ln\frac{4\,r_2}{b}\right) \quad\cdots\cdots\cdots (13 \cdot a)$$

$$b^2 = \frac{8\,r_1 r_2}{\pi(r_1 + r_2)}\left(\frac{1-\nu^2}{E}\right)q \quad\cdots\cdots\cdots (13 \cdot b)$$

Then, K_n is given in eq. (14).

$$k_n = \frac{q}{\delta} = \frac{\pi E}{2(1-\nu^2)(1.5 + 2\ln(4\,r/b))} \quad\cdots\cdots\cdots (14)$$

K_s is determined in eq. (15) by introducing a reduction rate, β.

$$K_s = \beta K_n \quad\cdots\cdots\cdots (15)$$

Damping coefficients are determined from eqs. (16) and (17).

$$\eta_n = 2\sqrt{mk_n} \quad\cdots\cdots\cdots (16)$$

$$\eta_s = \eta_n\sqrt{\beta} \quad\cdots\cdots\cdots (17)$$

  m : Mass of a particle

  η_n : Damping coefficient between particles in the normal direction

  η_s : Damping coefficient between particles in the tangential direction.

Values of the above coefficients when the particle is sand are

(Density) = 2.7 (tf/m³), $\nu = 0.3$, $E = 1.42 \times 10^6$ (tf/m²)

$K_n = 1.4 \times 10^9$ (N/m), $\eta_n = 2.2 \times 10^2$ (N s/m)

Assuming $\beta = 0.25$,

$K_s = 3.5 \times 10^8$ (N/m), $\eta_s = 55$ (N s/m)

Cundall recommended the value of Δt in eq. (18) from the condition of convergence and the stability of the approximate solution for the finite difference equation ;

$$\Delta t < 2\sqrt{m/k_n} \quad\cdots\cdots\cdots (18)$$

Substitution of the above values of K_n, in eq. (18), gives a value of Δt less than 2.8×10^{-7} (s), too small to use in calculating the simulation within a moderate CPU time. We therefore used comparatively smaller values for K_n and K_s ; $K_n = 1.4 \times 10^6$ (N/m), and $K_s = 3.5 \times 10^5$ (N/m), which gave a value for Δt of 1×10^{-6} (s).

4. ANALYSIS OF LIQUEFACTION CAUSED BY EARTHQUAKE

(1) Method of analysis

The assembly model is roughly divided into two parts (Fig. 5). One is the assembly for the frame work, two walls and a bottom; the other is the internal particle assembly. The particle frame work permits water to pass for drainage with the permeability coefficient K_3.

The values of the excessive pore pressure on the surface of the assembly and the outside the wall is zero. Horizontal shear deformation appears only on the wall. At the bottom no deformation occurs. The shear and normal springs and dashpots are shown in Fig. 6(a) and (b).

Fig. 7 shows why the particles inside the wall have gaps between them. Actual sand particles are not round; they have irregular corners. But, when they move because of an external force, these irregular edges are eroded, and the particles become rounded. In the model assembly given in Fig. 5, the number of edge particles is 47 and internal particles 192. The initial normal force distribution of these particles is shown in Fig. 8. The mechanical properties of a spring between particles is nonlinear (Fig. 9). Dense ground indicates elastic properties and loose ground non-linear properties.

Data used in the analysis (Tables 1-3) are explained as follows. The input earthquakes to the frame work of the assembly are the sinusoidal motion and El Centro types. As stated, the time interval, Δt, of the computation is so very short, 1.0×10^{-6} s, that the longest actual period of analysis is only 0.2 s. We adopted a sinusoidal wave of 1 800 gal, 50 Hz, and changed the El Centro wave by a corresponding rate.

(2) Numerical results

Examples of the simulation results for Case 1 (Saturated, Undrained) are shown in Fig. 10 (Location, Velocity, Normal force of particles) and in Fig. 11 (Excessive pore pressure). These results show that particle location did not change so much. The velocity distribution shows that most of the particles moved downward at $t=0.01$ s, but their downward movement was stopped because of the increase in excessive
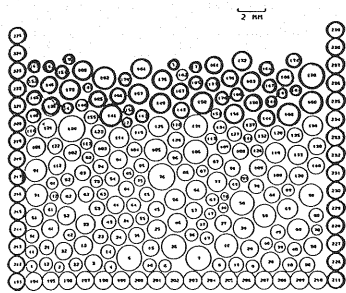

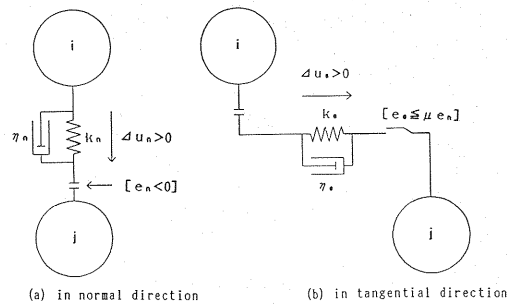Fig. 5 Location of particles (Saturated, Initial condition).

(a) in normal direction   (b) in tangential direction

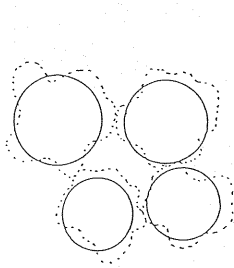Fig. 6 The spring and viscous dashpots between particles.

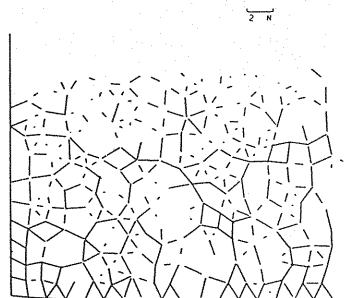Fig. 7 Idealization of actual sand particles (dotted shape) to solid circular particles.

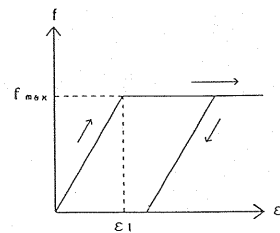Fig. 8 Normal forces (Saturated, Initial condition).

Fig. 9 Nonlinear characteristics of the spring between particles.

Table 1   Conditions of simulation cases.

Case	Water	Spring in normal direction	Input acceleration
1	Saturated Undrained	Nonlinear Inelastic	Sine Wave
2	Dry		
3	Saturated Drained		
4	Saturated Undrained	Elastic	
5	Dry		
6	Saturated Undrained	Nonlinear Inelastic	El Centro earthquake wave
7	Dry		

Table 2   Value of coefficients for numerical simulation.

Elastic Spring Coefficient of Particle in Normal Direction	K_n	1.4×10^5	(N/m)
Damping Coefficient of Particle in Normal Direction	η_n	2.6	(N·S/m)
Elastic Spring Coefficient of Particle in Tangential Direction	K_s	3.5×10^4	(N/m)
Damping Coefficient of Particle in Tangential Direction	η_s	6.0×10^{-1}	(N·S/m)
Elastic Spring Coefficient of Wall in Tangential Direction	K_s'	1.5×10^5	(N/m)
Damping Coefficient of Wall	η_s'	6.0×10^{-1}	(N·S/m)
Density of Particle	ρ	2.7×10^3	(kg/m²)
Density of Water	ρ_w	1.0×10^3	(kg/m²)
Young's Modulous of Water	E_w	2.4×10^3	(N/m)
Time Interval for Calculation	Δt	1.0×10^{-6}	(s)

Table 3   Value of permeability coefficient.

(s⁻¹)

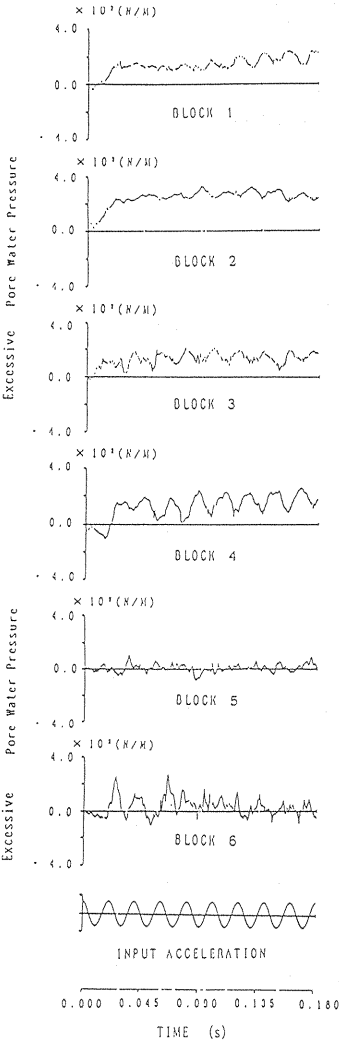| CASE	k1	k2	k3
1,4,6	1.0×10^3	1.0×10^2	0.0
3	1.0×10^5	1.0×10^4	1.0×10^4

Fig. 11   Time history of excessive pore water pressure (Saturated, Undrained).
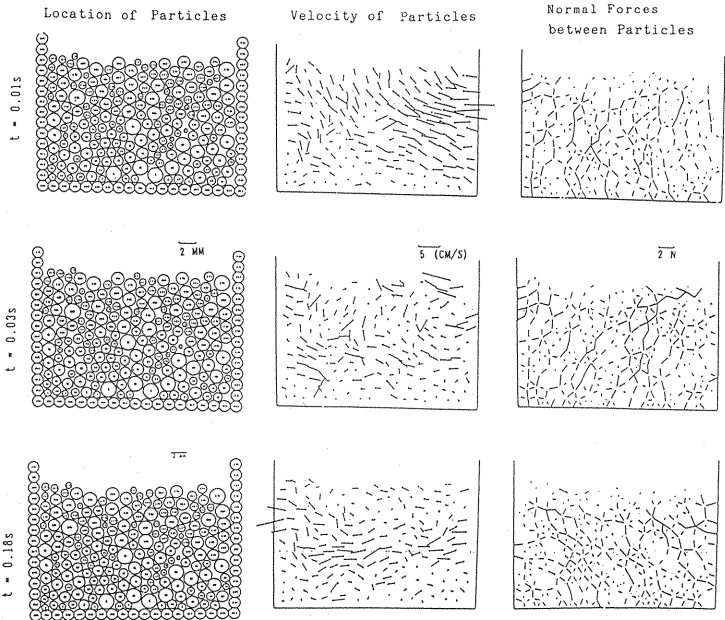

Fig. 10   Particles response under horizontal sinusoidal shaking (Saturated, Undrained condition).

pore pressure. Thereafter, they repeated almost periodic movement. Normal forces tend to decrease with time, especially, in the lower part. Excessive pore pressure has two main components ; a dynamic pressure, almost the same as the input acceleration and a gradually increasing DC component.

In blocks Nos. 5 and 6, (the block numbers, are given in **Fig. 12**) which are close to the surface, the DC component of the pressure is almost zero because it dissipates upward from the surface. In the other blocks the DC components gradually increase and approach the liquefied state.

The results for Case 2 (Dry condition) which correspond to those for Case 1 (Saturated condition) are shown in **Fig. 13**. Most particles subsided and their packing became more dense because there was no pore water between the particles and no uplifting force acted on them. The results of excessive pore pressure for Case 3 (Saturated, Drained) are shown in **Fig. 14**. The particles idealized in Case 3 are gravels having larger diameters than sand because a fairly large value for the permeability coefficient was considered. Pore pressure was almost zero in all the blocks.

Changes in the porosity of the particles in Cases 1 to 3 are shown in **Fig. 15**. Assembly under the saturated and undrained condition is characterized by less volume change, while the porosity decreases with time a little. Porosity decreases with time in the dry condition but shows an intermediate character in the saturated and undrained condition. These results confirm that a decrease in normal stress (effective stress) and a subsidence of
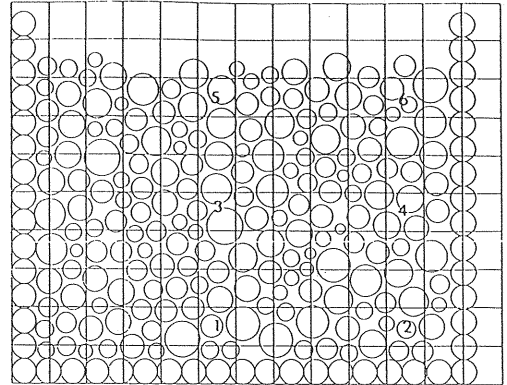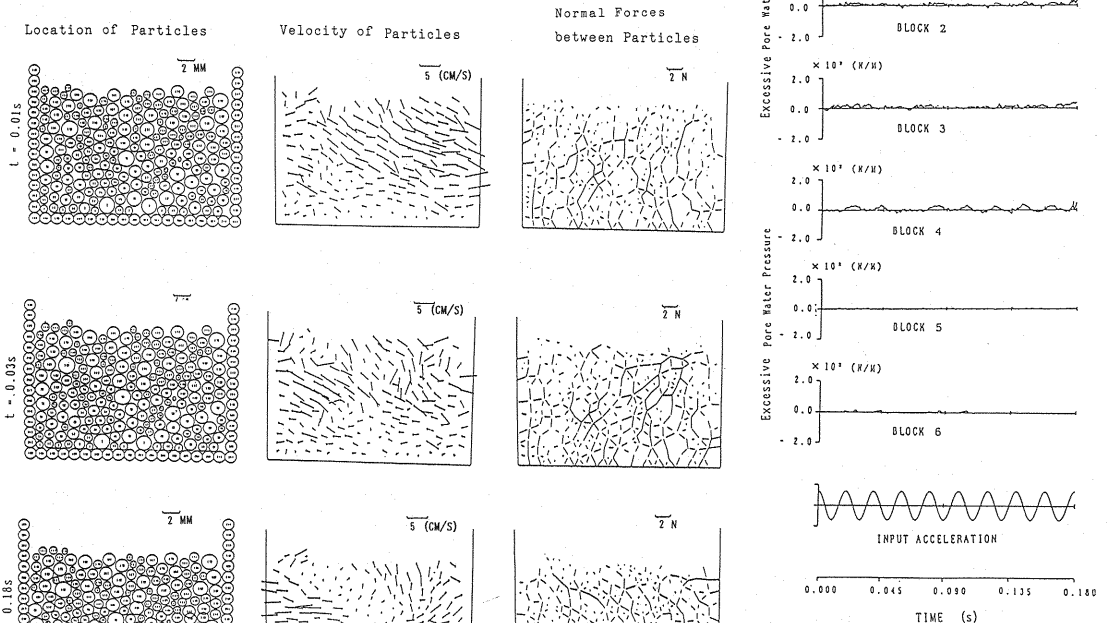
Fig. 12 Numbering of blocks.

Fig. 13 Particles response under horizontal sinusoidal shaking (Dry condition).

Fig. 14 Time history of pore water pressure (Saturated, Drained, Inelastic hysteretic spring).
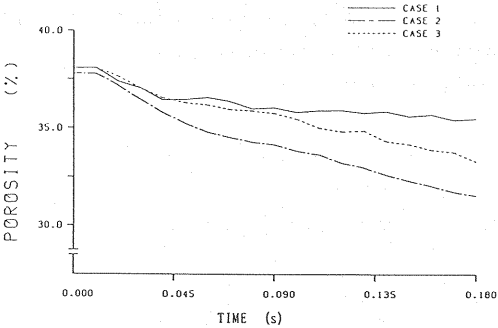
Fig. 15 Time history of porosity of particles (Sinusoidal shaking, Nonlinear hysteretic spring).
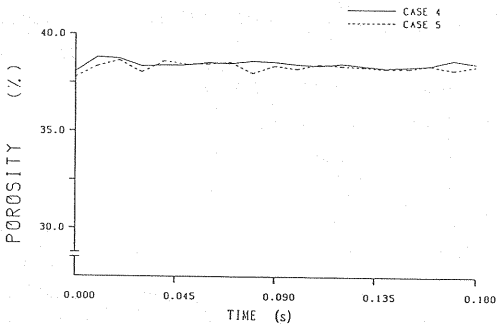

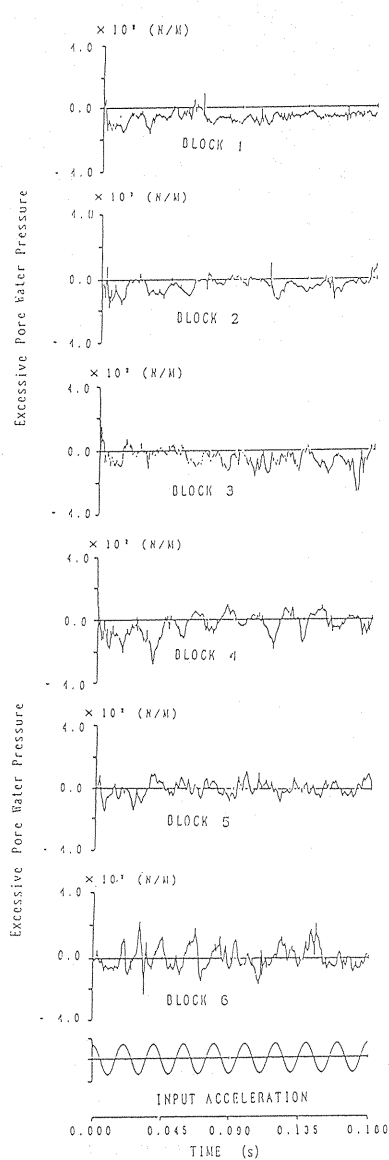Fig. 16 Time history of the particles porosity (Sinusoidal shaking, Elastic spring).

Fig. 17 Time history of pore water pressure (Saturated, Undrained, Elastic spring).
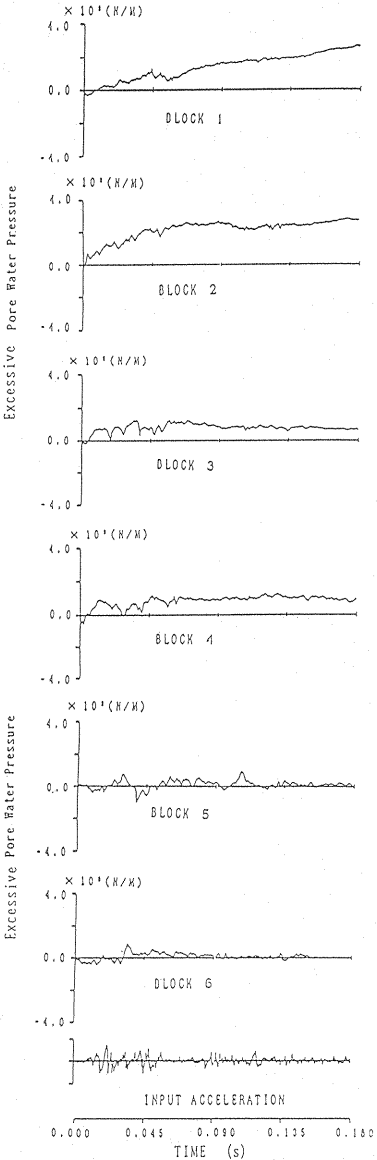

Fig. 18 Time history of pore water pressure (Saturated, Undrained, Inelastic hysteretic spring).

particles at the time of shearing take place because of a rise in the excessive pore pressure for the saturated and undrained condition.

Changes in porosity for Cases 4 and 5 is shown in Fig. 16, and changes in the excessive pore pressure in Fig. 17. The characteristics of the springs in these two cases are complete elasticity and a correspondence to dense sand. The pore ratio for particles under saturated-undrained or dry conditions shows almost no change. The pore pressure under the saturated undrained condition fluctuates around the zero line in each block and sometimes becomes negative. There is no accumulation of pore pressure.

The input force in Cases 6 and 7 is the EL Centro earthquake wave. The behavior of excessive water pressure in Case 6 (Saturated, Undrained) is shown in Fig. 18. Similar water pressure behavior as that in case 7 is seen for the EL Centro earthquake case. Fig. 19 shows the velocity distribution and Fig. 20 the change in porosity of dry particles due to earthquake input. There is no difference in the behavior of particles subjected to a sinusoidal input or to an earthquake type input.

5. CONCLUSIONS

We used nonlinear spring in the normal direction between particles to express "Dilatancy" in our two-dimensional treatment. The excessive pore pressure in our numerical results rose gradually due to the effect of shaking. This result agrees with results of past laboratory tests. Contact among neighboring particles did not disappear even under high pore pressure; consequently, the phenomenon of complete liquefaction was not realized. Complete liquefaction can be determined only by three dimensional analysis. As it needs much more computing time, we must wait for an advanced and faster computer.

All computations were made with the HITAC M 280 H computer (17 MFlops, 32 MB) at the Earthquake Research Institute of the University of Tokyo.
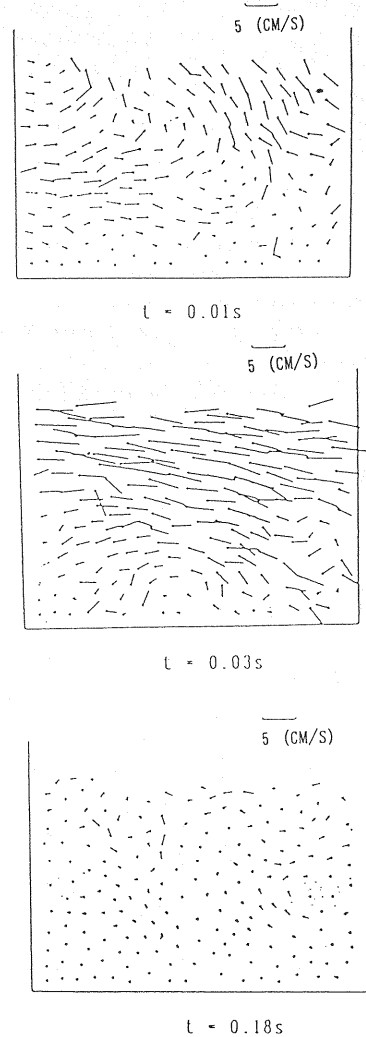

t = 0.01 s

t = 0.03 s

t = 0.18 s

Fig. 19 Velocity of particles under horizontal earthquake ground motion (Dry particles).
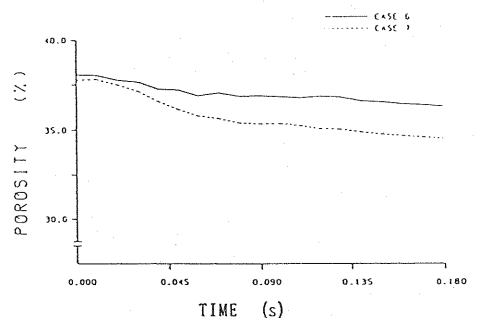
Fig. 20 Time history of particles porosity (Earthquake shaking. Nonlinear hysteretic spring).

REFERENCES

1) Mogami, T. : A Statistical Approach to the Mechanics of Granular Materials, Soil and Foundation, Vol. 5, No. 2, pp. 26~36, 1965.

2) Cundall, P. A. : A Computer Model for Simulating Progressive, Large Scale Movement in a Blocky Rock System, Symp. ISRM,

Nancy, France, Proc., Vol. 2, pp. 129~136, 1971.

3) Hakuno, M. and Hirao, T. : A Trial Related to Random Packing of Particle Assemblies, Proc. of JSCE, No. 219, pp. 55~63, 1973 (in Japanese).

4) Kiyama, H., Fujimura, H. and Nishimura, T. : On Analyzing Settlement of the Ground Surface Owing to Tunnel Excavation with Cundall's Model, Annual meeting of Japan Society of Civil Engineers, 3, pp. 309~310, 1982 (in Japanese).

5) Kiyama, H. and Fujimura, H. : The Analysis of the Gravity Flow of Rock Granular Assemblies using Cundall's Model, Proc. of Japan Society of Civil Engineers, No. 333, pp. 137~146, 1983 (in Japanese).

6) Uemura, D. and Hakuno, M. : Granular Assembly Simulation using Cundall's Model for the Dynamic Collapse of the Structural Foundation, Structural Engineering/Earthquake Engineering, Vol. 4, No. 1, 155 s~164 s (Proc. of JSCE, No. 380), Japan Society of Civil Engineers, 1987.

7) Izutsu, H., Kiyama, H., Fujimura, H. and Nishimura, T. : DEM Analysis Taking into Account the Behavior of Pore Water, Proc. 21th annual meeting of the Japanese Society of Soil Mechanics and Foundation Engineering, pp. 1621~1622, 1986 (in Japanese).

8) Kishino, Y. : Disc Model Analysis of Granular Media, Preprint of the US-Japan Seminar : Micromechanics of Granular Materials, pp. 146~155, 1987, Sendai, Japan.

9) Tarumi, Y. and Hakuno, M. : A Granular Assembly Simulation for the Liquefaction of Sand and Quicksand, Bulletin of Earthquake Research Institute, University of Tokyo, Vol. 62, pp. 535~577, 1987 (Japanese with English abstract).